A unique potential to study scattering and fusion phenomena in heavy ion collisions around Coulomb barrier

Bidhubhusan Sahu[1,*], **Kamala Kanta Jena**[2], **Santosh Kumar Agarwalla**[3]
Department of Physics, School of Applied Sciences, KIIT Deemed to be University, Bhubeneswar-751024, Odisha, India
[2]P. G. Department of Physics, Bhadrak Autonomous College, Bhadrak-756100, India
[3]Department of Applied Physics and Ballistics, Fakir Mohan University, Balasore-756019, India
[*]Email: bbsahufpy@kiit.ac.in, kkjena1@gmail.com, san1612@rediffmail.com

Abstract: To examine the data of angular variation in elastic scattering cross sections, a systematic recursive formula of the partial-wave scattering matrix for the total effective complex potential of nucleus-nucleus collisions is developed. The cross sections for the absorption from arbitrarily small intervals are also expressed in an additional manner. This results in an assessment of the absorption contributions in the interior region of the effective potential, which explains the fusion cross section (σ_{fus}) data for different incident center-of-mass energies $E_{c.m.}$. The interaction potential taken into account in this study is energy independent and enables resonance states in various partial-wave trajectories owing to its weakly absorbing characteristic. Therefore, it becomes clear that the occurrence of these resonances is the physical cause of the observable oscillatory structure in the modification of the quantity $D(E_{c.m.})$, the second derivative of the product "$E_{c.m.}\sigma_{fus}$" with respect to $E_{c.m.}$. In this chapter, we discuss simultaneous and extremely effective descriptions of the cross sections for fusion, elastic scattering, and the outcomes of $D(E_{c.m.})$ in various kinds of heavy-ion collisions.

1 Introduction

There have been numerous experiments on the nucleus-nucleus collision process, and extensive data on the angular distribution of elastic scattering ($\frac{d\sigma(\theta)}{d\sigma_R(\theta)}$) at various incidence energies and fusion cross sections at firmly energy intervals are now available [1]− [5]. Eight such systems come to mind in this regard: ^{12}C+^{208}Pb in Refs. [1, 3], ^{16}O+^{208}Pb in Refs. [2, 4], ^{19}F+^{208}Pb in Refs. [6, 7], ^{16}O+^{144}Sm in Refs. [8–10], and ^{16}O+^{62}Ni in Refs. [11, 12] all of which include a wealth of information. Unlike in light ion systems, the shape resonances generated by the effective potential in heavy ion systems, though present, are hardly observable experimentally [13]. Further research is needed to ascertain the potential impact and expression of such resonances in any other visible forms throughout the collision process. One employs the phenomenological potential, which is often complicated, to analyse these heavy ion collision data. The observed values of the elastic scattering cross section at different energies are fitted to determine all the parameters defining the potential. Using the same interaction potential, one has to explain the fusion cross-section (σ_{fus}) data arising from the fusion process and resonance phenomena occurring via elastic scattering process of the colliding nuclei. It is challenging to discover a special potential that can address both of these phenomena at the same time since the scattering process is sensitive to the nature of the potential on the surface region and the fusing process is an internal activity. Additionally, once the elastic scattering data has been obtained for the theoretical analysis, one can easily obtain the results of the total reaction cross section (σ_r), which includes the cross section for various reaction channels, with the fusion channel predominating in low energy collision activities. Now, a problem arises in extracting the part of reaction cross section from the the total σ_r which can exactly account for the measured data of σ_{fus}.

The expected value of the imaginary component of the potential, calculated using the distorted waves from the full potential in the elastic channel, accounts for σ_r within the scope of optical potential model analysis of scattering. This could be easily interpreted as the total of the cross sections caused by absorption in the various areas of the potential where the imaginary component is actively present. Using the same wave function that describes the elastic scattering data, one can obtain the absorption cross section σ_A^i in the infinitesimally small ith radial interval δr^i giving the total absorption cross section $\sigma_A = \sum_{i=1}^{n} \sigma_A^i$ where n is the total number of intervals such that the total range of the potential R= $\sum_{i=1}^{n} \delta r^i$. It is relatively simple to express clearly the quantity of absorption over different regions or intervals of the potential using this equation for absorption. One anticipates that the absorption in this spatial area $0 < r < R_B$ has to account for the experimental results of the fusion cross section (σ_{fus}^{expt}) based on the idea that the fusion of two nuclei happens in the region internal to the radial location (R_B) of the electrostatic Coulomb barrier. The exact radius R_{fus} up-to which absorption cross section is to be calculated to explain σ_{fus}^{expt} is known as fusion radius. This concept of fusion cross section has been used in the direct reaction model (DRM) of Udagawa et al. [14, 15]. However, they have estimated the value of R_{fus} larger than the corresponding value of R_B in most of the heavy ion systems analyzed thereby

asking fusion to initiate before crossing the Coulomb barrier. This is contrary to the popular assumption [16, 17] that fusion only takes place after the barrier has been fully penetrated and hence, this result has attracted severe criticism in the literature [18, 19].

In our present calculation, we overcome this problem and explain results of σ_{fus}^{expt} in the cases of ^{12}C+^{208}Pb, ^{16}O+^{208}Pb, ^{19}F+^{208}Pb, ^{16}O+^{144}Sm, and ^{16}O+^{62}Ni systems with value of R_{fus} parameter always less than the value of R_B in a given system. Instead of employing Runge-Kutta or other comparable methods of numerical integration, we use an alternative approach to solve the Schrödinger equation for a given nucleus-nucleus potential. Our approach is appropriate for the investigation of region-wise absorption in the reaction process. We simulate the potential in our computation using arbitrarily tiny rectangular pieces, and we establish an analytical formula for the scattering matrix (S-matrix), which is utilized to explain the elastic scattering data, by employing accurate wave functions and their analytical continuation between neighboring parts. The quantity of absorption in each tiny portion (width) of the potential is determined using the same wave functions. It turns out that the overall reaction cross section σ_r is equal to the sum of all contributions for absorption across the whole range of potential. In contrast, we take into consideration the total of the contributions for absorption across a constrained region $0 < r < R_{fus}$ inside the radial location R_B of the Coulomb barrier in order to explain why the value of the fusion cross section σ_{fus} is always less than that of σ_r. We've confirmed that the outcomes of elastic scattering obtained using our approach and the Runge-Kutta method are identical.

In the collision of two heavy nuclei with incidence energies close to the Coulomb barrier, measurements with excellent accuracy reveal data of σ_{fus} at relatively close energy intervals. When heavy pairs of nuclei collide, the variation of the outcomes of σ_{fus} with the bombarding center of mass energy $E_{c.m.}$ seems smooth fluctuating without any distinctive characteristic or structure, but it oscillates when light pairs of nuclei collide. But, when the product $E_{c.m.}\sigma_{fus}$ is differentiated twice with respect to $E_{c.m.}$ using some point difference formula, the corresponding result of $D(E_{c.m.})$=$\frac{d^2(E_{c.m.}\sigma_{fus})}{dE_{c.m.}^2}$, generally referred to as barrier distribution, exhibits peculiar oscillatory structure in its variation with $E_{c.m.}$ [5]. The corresponding experimental results of $D(E_{c.m.})$ in the cases of the above eight systems are explained with remarkable success in addressing the peak structure. The theoretical results of σ_{fus} obtained in our above method of region-wise absorption at various incident $E_{c.m.}$ are presented in the form of $D(E_{c.m.})$. In this study, we identify the following crucial traits in the potential that we used; in addition to being very deep and having little diffuseness, the real part is also highly strong compared to the imaginary part. Shape resonance states (experimentally unseen) [13] might endure throughout the collision process as a result of the formation of standing waves in the nuclear well because of the potential's less absorptive character. The oscillating structure in the results of $D(E_{c.m.})$ as a function of $E_{c.m.}$ is consequently attributed to these resonances.

It should be noted that coupled-channels (CC) formulation is the natural language for investigating fusion processes at energies around the Coulomb barrier. For this, a number of computer programmes, including CCFUS [20,21] and CCFULL [22], have been created. Since there are many channels present in the heavy ion collision process due to its complexity, solving coupled equations that take all of these channels into account is both difficult and time-consuming. Such formulations are, however, somewhat schematic and include important approximations to ease the process of calculations. No matter how exhaustive the CC calculation is, it has been noted [4] that simultaneous explanation of the aspects of both σ_{fus} and $D(E_{c.m.})$ in the majority of pairings of nuclei is far from the satisfactory. This unsatisfactory circumstance is still present in the most current CC projections [23] based on M3Y plus repulsion potential used to analyze the data of the ^{16}O+^{208}Pb system. According to a most recent calculation [24], even the observed data of σ_{fus} alone from the deep sub-barrier area to the above barrier region of energy cannot be concurrently reproduced by the CC calculations with the identical Woods-Saxon nuclear potential. The microscopic CC calculation is essentially a one-dimensional barrier passing model [25, 26] that includes lots of barriers with different heights that are produced as a result of coupling between the relative motion and the internal degrees of freedom of the colliding nuclei, such as static deformation, collective vibration [27], inelastic excitation, and nucleon transfer [23]. In order to enforce an ingoing-wave boundary condition for the barrier crossing model, the CC calculation for the fusion cross section does not take the influence of any mechanism produced by the interaction potential in the interior pocket area into account because it is thought to be extremely absorptive.

The nucleus-nucleus potential in the interior or pocket area is a key component of the current formulation and is used to explain the experimental results of σ_{fus} as well as the related function $D(E_{c.m.})$ generated from measured σ_{fus}. Due to the pocket's less absorptive character, the resonances that it produces successfully depict the oscillatory structure of $D(E_{c.m.})$. Furthermore, although it is not stated directly in our model, the impact of coupling is implied. It is anticipated that the entrance channel potential barrier would vary dramatically when a non-elastic channel is coupled with it [28], especially in the interior region $r < R_B$, where the effective potential will suddenly drop [29,30]. By choosing a low value for the diffuseness parameter in the Woods-Saxon form of nuclear potential, this coupling effect may be easily included in the formulation. The current formulation includes the influence of channel coupling in a phenomenological fashion by using such a modest diffuseness value in the simultaneous analysis of elastic scattering and fusion cross section data. In section 1.2, we present the formulation for analytical expression for S-matrix

and region-wise absorption. Application of the formulation is done in section 1.3 to the analysis of experimental data of $\frac{d\sigma(\theta)}{d\sigma_R(\theta)}$, $\sigma_{fus}(E_{c.m.})$ and $D(E_{c.m.})$ in the cases of ^{12}C+^{208}Pb, ^{16}O+^{208}Pb, ^{19}F+^{208}Pb, ^{16}O+^{144}Sm, and ^{16}O+^{62}Ni systems. We summarize the results in section 1.4.

2 Formulation

In the nuclear optical model, which is frequently employed in the study of heavy ion collisions, the solution of the radial Schrödinger equation for a complex Coulomb nuclear potential is the most significant component of the scattering and reaction cross section. The complex nuclear potential (V_N(r)), electrostatic or Coulomb potential (V_C(r)), and the centrifugal component (V_ℓ(r)) are added to provide the effective potential in the radial equation. When solving the Schrödinger equation for this potential, it is most common to use the Runge-Kutta (RK) type method of numerical integration to obtain the wave function and its derivative at a radial point outside the range of the nuclear potential. This wave function and derivative are then connected to the exact Coulomb wave function and its derivative to obtain the results of the scattering matrix for the analysis of scattering data, etc. However, with this procedure, it is not simple to separate a portion of the reaction cross-section from the entire reaction cross-section to analyze the fusion cross-section. As a result, we use a practical but slightly different method to resolve the Schrödinger equation [31–33].

Let's start by carefully examining the s-wave scattering. A chain of 'n' rectangular potentials with arbitrary small widths 'w' can be thought of as a potential U(r). In reality, a similar process is implied in any numerical integration of a differential equation. Having simulated the potential up to a maximum range r=R$_{max}$, we have R$_{max}$=$\sum_i^n w_i$ where w_i=w is the width of ith rectangle.

Let, in the jth region, $\sum_{i=1}^{j-1} w_i < r \leq \sum_{i=1}^{j} w_i$, the strength and width of the potential be denoted by U_j and w_j, respectively. The reduced Schrödinger equation in this region is

$$\frac{d^2\Phi(r)}{dr^2} + \frac{2m}{\hbar^2}(E - U_j)\Phi(r) = 0, \tag{1}$$

with the following solution

$$\Phi_j(r) = a_j e^{ik_j r} + b_j e^{-ik_j r}, \tag{2}$$

where the wave number k_j is defined as $k_j = \sqrt{\frac{2m}{\hbar^2}(E - U_j)}$ for the jth segment of width w_j. For two adjacent segments, we use the notation $q_{ji} = -q_{ij} = \frac{k_j - k_i}{k_j + k_i}$. Here, m denotes the particle's mass and E denotes the incident energy. The solution in the first three segments, which are near the origin and $r = 0$, may be expressed explicitly as;

$$\Phi_I = \sin k_1(r - c_1), \quad 0 < r < w_1 \tag{3}$$

$$\Phi_{II} = a_2 e^{ik_2(r-c_2)} + b_2 e^{-ik_2(r-c_2)}, \quad w_1 < r < (w_1 + w_2) \tag{4}$$

$$\Phi_{III} = a_3 e^{ik_3(r-c_3)} + b_3 e^{-ik_3(r-c_3)}, \quad (w_1 + w_2) < r < (w_1 + w_2 + w_3) \tag{5}$$

Here, a_2, b_2, a_3, and b_3 stand for the coefficients of the wave functions and c_1, c_2 and c_3 indicate some arbitrary constants.

Matching the wave functions and the derivatives at the boundary at $r = w_1$, we get

$$a_2 = \frac{1}{2} e^{-ik_2(w_1 - c_2)} \Big[\sin k_1(w_1 - c_1) + \frac{k_1}{ik_2} \cos k_1(w_1 - c_1) \Big], \tag{6}$$

$$b_2 = \frac{1}{2} e^{ik_2(w_1 - c_2)} \Big[\sin k_1(w_1 - c_1) - \frac{k_1}{ik_2} \cos k_1(w_1 - c_1) \Big], \tag{7}$$

$$\frac{a_2}{b_2} = e^{-2ik_2(w_1 - c_2)} \times q_{21} \ , \tag{8}$$

where

$$q_{21} = \frac{\sin k_1(w_1 - c_1) + \frac{k_1}{ik_2} \cos k_1(w_1 - c_1)}{\sin k_1(w_1 - c_1) - \frac{k_1}{ik_2} \cos k_1(w_1 - c_1)}. \tag{9}$$

Similar calculation at the boundary at $r = w_1 + w_2$ yields

$$a_3 = \frac{1}{2} e^{-ik_3(w_1+w_2-c_3)} b_2 e^{-ik_2(w_1+w_2-c_3)} \Big[(1 - \frac{k_2}{k_3}) + (1 + \frac{k_2}{k_3}) e^{2ik_2 w_2} q_{21} \Big], \tag{10}$$

$$b_3 = \frac{1}{2} e^{ik_3(w_1+w_2-c_3)} b_2 e^{-ik_2(w_1+w_2-c_3)} \Big[(1 + \frac{k_2}{k_3}) + (1 - \frac{k_2}{k_3}) e^{2ik_2 w_2} q_{21} \Big], \tag{11}$$

$$\frac{a_3}{b_3} = e^{-2ik_3(w_1+w_2-c_3)} \times q_{321} \ , \tag{12}$$

where

$$q_{321} = \frac{q_{32} + q_{21}\, e^{2ik_2 w_2}}{1 + q_{32} \times q_{21}\, e^{2ik_2 w_2}} \tag{13}$$

and

$$q_{32} = \frac{k_3 - k_2}{k_3 + k_2}. \tag{14}$$

This can be generalized for n boundaries to give

$$\frac{a_n}{b_n} = e^{-2ik_n(\sum_{j=1}^{n-1} w_j - c_n)} \times q_{n,n-1,n-2,\ldots 1}, \tag{15}$$

$$q_{n,n-1,n-2,\ldots 1} = \frac{q_{n,n-1} + q_{n-1,n-2,\ldots 1} e^{2ik_{n-1}w_{n-1}}}{1 + q_{n,n-1} \times q_{n-1,n-2,\ldots 1} e^{2ik_{n-1}w_{n-1}}}, \tag{16}$$

$$\vdots$$

$$q_{21} = \frac{\sin k_1(w_1 - c_1) + \frac{k_1}{ik_2} \cos k_1(w_1 - c_1)}{\sin k_1(w_1 - c_1) - \frac{k_1}{ik_2} \cos k_1(w_1 - c_1)} \ , \tag{17}$$

where, $q_{n,n-1} = \frac{k_n - k_{n-1}}{k_n + k_{n-1}}$.
Setting the arbitrary constants as $c_1 = w_1$ and
$c_n = \sum_{j=1}^{n-1} w_j$,
we get

$$D^{(0)} = \frac{a_n}{b_n} = q_{n,n-1,n-2,\ldots 1} = \frac{q_{n,n-1} + q_{n-1,n-2,\ldots 1} e^{2ik_{n-1}w_{n-1}}}{1 + q_{n,n-1} \times q_{n-1,n-2,\ldots 1} e^{2ik_{n-1}w_{n-1}}}, \tag{18}$$

with

$$q_{n-1,n-2,\ldots 1} = \frac{q_{n-1,n-2} + q_{n-2,n-3,\ldots 1} e^{2ik_{n-2}w_{n-2}}}{1 + q_{n-1,n-2} \times q_{n-2,n-3,\ldots 1} e^{2ik_{n-2}w_{n-2}}}, \tag{19}$$

$$\vdots$$

$$q_{21} = -1. \tag{20}$$

The function in the m-region may be defined in terms of that in the (m-1) area using the recursive nature of the formula for $q_{n,n-1,n-2,\ldots 1}$. This allows us to simulate the potential U(r) by n-step potentials and create an easy-to-use numerical program for the assessment of the scattering matrix and the wave function at a certain incident energy. If $\sum_{i=1}^{n} w_i = R_n = R_{max}$, such that the potential $U_j(r)$ considered in 1 is zero for $r > R_n$, it can be easily understood that the s-wave S-matrix is given by $S_0 = -\frac{a_n}{b_n}$ and the total absorption or reaction cross section in the region $0 < r < R_n$ is given by

$$\sigma_{abs}^{(0)} = \frac{\pi}{k^2}(1 - \frac{|a_n|^2}{|b_n|^2}).$$

Similarly, $S_0^p = -\frac{a_p}{b_p}$ can be interpreted as the S-matrix of the original potential truncated at $R_p(= \sum_{i=1}^{p} w_i) < R_{max}$. Hence, $\frac{\pi}{k^2}(1 - \frac{|a_p|^2}{|b_p|^2})$ can be taken as the absorption cross section generated in the region $0 < r < R_p$. Thus, $\frac{\pi}{k^2}[(1 - \frac{|a_p|^2}{|b_p|^2}) - (1 - \frac{|a_q|^2}{|b_q|^2})]$ shall give the contribution to the absorption cross section from the region $R_p > r > R_q = \sum_{i=1}^{q} w_i$.

Taking the complex conjugate of the Schrödinger equation (1) and rearranging, we get

$$2ik_n(\mid a_n \mid^2 - \mid b_n \mid^2) = \int_0^{R_n} 2iIm\, U(r)\ \Phi\Phi^*\ dr, \tag{21}$$

$$1 - \frac{\mid a_n \mid^2}{\mid b_n \mid^2} = I_1 + I_2 + \ldots, \tag{22}$$

$$I_1 = -\frac{1}{k_n}\int_0^{w_1} Im\, U(r) \mid \frac{\Phi}{b_n} \mid^2\ dr, \tag{23}$$

$$I_2 = -\frac{1}{k_n}\int_{w_1}^{(w_1+w_2)} Im\, U(r) \mid \frac{\Phi}{b_n} \mid^2\ dr. \tag{24}$$

Using the respective wave function and the potential in a given segment, we simplify the corresponding integral and obtain

$$1 - \frac{\mid a_n \mid^2}{\mid b_n \mid^2} = \sum_{j=1}^{n} I_j, \tag{25}$$

with

$$R_n = \sum_{j=1}^{n} w_j = R_{max}. \tag{26}$$

Considering same width for all segments, i.e. $w = w_1 = w_2 = w_3 = \ldots$, we have $n = \frac{R_{max}}{w}$.
This result in the jth segment can be expressed as

$$I_j = (-\frac{1}{k_n})\frac{ImU_j}{\mid b_n \mid^2}\Big[\frac{\mid b_j \mid^2}{2Imk_j}e^{-2Imk_j\ w_{j-1}}(e^{2Imk_j\ w_j} - 1) - \frac{\mid b_j \mid^2}{2Imk_j}e^{2Imk_j\ w_{j-1}}(e^{-2Imk_j\ w_j} - 1) + \frac{1}{Rek_j}Im\Big(a_j b_j^* e^{2Imk_j\ w_{j-1}}(e^{2iRek_j\ w_j} - 1)\Big)\Big]. \tag{27}$$

The asterisk indicates the complex conjugate of the respective quantity. The procedure for calculation of S-matrix through Eqs. (4.18) - (4.20) with multistep potential (MP) approximation makes the procedure an algebraic recursive method which can be easily programmed. The Eqs. (4.27) - (4.29) give a method to study the absorption cross section as discrete sums of contributions from various sections.

It is simple to generalise this method to the challenging heavy ion Coulomb nuclear issue for any partial waves. One may use the MP approximation approach mentioned above for this effective potential to handle the problem of higher partial waves as the scattering by V_N(r)+V_C(r)+ V_ℓ(r). The complexity of the $r^{\ell+1}$ behaviour of the wave function very near the origin in the complex potential scattering is not particularly important for the following reasons. The properly normalized wave function typically attenuates quickly to zero well beyond the origin in the case of complex absorptive potential due to the existence of absorption. As a result, one may begin the S-matrix computation well after r=0, where the multistep approximation is fairly precise. We have confirmed that the cross-section and S-matrix findings produced by our strategy are nearly identical to those produced by traditional methods.

In the region $0 < r \leq R_{max}$, the potential consists of all the three parts V_N(r), V_C(r) and V_ℓ(r). But in the outer region $r \geq R_{max}$, the potential of the nucleus-nucleus interaction is only Coulombic (V_C(r)) with the centrifugal terms V_ℓ(r)=$\frac{\hbar^2}{2m}\frac{\ell(\ell+1)}{r^2}$ for different angular momentum partial wave ℓ.

Using the exact Coulomb wave functions i.e. G_ℓ and F_ℓ and their derivatives G'_ℓ and F'_ℓ, in the outer region $r \geq R_{max}$ and the wave function $\Phi_n(r) = a_n e^{ik_n r} + b_n e^{-ik_n r}$ and its derivative $\Phi'_n(r)$ in the left side of $r = R_{max}$, and matching them at

$r = R_{max}$, we get the expression for partial wave S-matrix η_ℓ as

$$\eta_\ell = 2iC_\ell + 1, \tag{28}$$

where

$$C_\ell = \frac{kF'_\ell - F_\ell H}{H(G_\ell + iF_\ell) - k(G'_\ell + iF'_\ell)}, \tag{29}$$

$$H = \frac{\Phi'_n}{\Phi_n} = ik_n \frac{D^{(\ell)}\ e^{ik_n R_{max}} - e^{-ik_n R_{max}}}{D^{(\ell)}\ e^{ik_n R_{max}} + e^{-ik_n R_{max}}}, \tag{30}$$

$$D^{(\ell)} = \frac{a_n}{b_n}, \tag{31}$$

with $k_n = \sqrt{\frac{2m}{\hbar^2}(E - V_n)}$ which is real at $r = R_{max}$, where the potential $V_n = V_C + V_\ell$ is real and $E > V_n$.

Using the above expression (4.30) for η_ℓ, we explain the elastic scattering of a given system. For the total reaction cross section one can use the formula

$$\sigma_r = \frac{\pi}{k^2} \sum_\ell (2\ell + 1)(1 - |\eta_\ell|^2) \tag{32}$$

As formulated above, this is equal to the absorption cross section

$$\sigma_{abs} = \frac{\pi}{k^2} \sum_\ell (2\ell + 1)(1 - \frac{|\ a_n\ |^2}{|\ b_n\ |^2}) = \frac{\pi}{k^2} \sum_\ell (2\ell + 1)(\sum_{j=1}^{n} I_j^{(\ell)}) \tag{33}$$

By taking into account the matching number of segments in the aforementioned summation, it is possible to determine the contribution of any component within the range $0 - R_{max}$ to the absorption or reaction cross section. With no potential disturbance, this calculation of region-wise absorption in the collision process yields the wave function that describes the angular distribution of elastic scattering data. If one wishes to obtain the amount of absorption cross section in the region $0 < r < R_{fus}$, where $R_{fus} < R_{max}$, the total number of segments to be considered in the summation (4.35) is $n_{fus} = \frac{R_{fus}}{w}$. The resulting cross section

$$\sigma_{fus} = \frac{\pi}{k^2} \sum_\ell (2\ell + 1)(\sum_{j=1}^{n_{fus}} I_j^{(\ell)}) \tag{34}$$

corresponds to the fusion cross section in the context of DRM [14], as mentioned in the introduction.

It might be beneficial at this point to briefly explore this MP formulation as a numerical approach. In comparison to the trapezoidal rule using straight-line sections, Simpson's rule using parabolic sections, and the spline technique using cubic polynomials, this method is, in a sense, the simplest approximation to the solution of the differential equation [34–36]. The latter techniques are highly helpful for computing the wave function with more accuracy, but they have the drawback of being difficult to describe algebraically in terms of simple intervals. The computation of wave function and cross-section up to three to four significant places of decimal, however, is fairly appropriate in the nuclear cross-section calculation given the experimental uncertainties involved. In a study [37], we compared the numerical results for typical potentials such Eckart and Ginocchio potentials produced using the MP technique in one dimension with those obtained using the RK and exact solution, and we discovered that the results agreed up to three significant places. This section has demonstrated how our analytical formulation results in a tidy recursive relation that makes it easier to calculate cross-sections and S-matrices. With this MP formulation, it is possible to transparently estimate the contribution to absorption in various potential segments and examine the nature of the wave function and its normalization. However, the wave function rises quickly in the calculations for the nucleus-nucleus optical model performed using the RK method [38] due to the imaginary potential and must be appropriately renormalized at various stages in order to perform the effective phase-shift calculations. This makes it more difficult to estimate the regional contributions to cross section and reactions [39]. In this chapter, we calculated the cross sections of elastic scattering and fusion in heavy ion collisions and successfully compared them with the corresponding experimental results to show the viability and applicability of this MP method in nuclear-scattering analysis. Standard optical model methods are used to confirm the numerical results of the elastic scattering cross sections that are reported in this chapter [38].

Table 1: Optical model potential parameters used in the calculations. V_B and R_B represent height and radial position of the Coulomb barrier, respectively.

System	V_N (MeV)	r_V (fm)	a_V (fm)	W (MeV)	r_W (fm)	a_W (fm)	r_C (fm)	V_B (MeV)	R_B (fm)	R_{fus} (fm)
^{12}C+^{208}Pb	125	1.31	0.320	3.0	1.325	0.25	0.90	56.7	12.16	9.9
^{16}O+^{208}Pb	125	1.35	0.285	2.0	1.320	0.15	1.02	73.7	12.52	8.8
^{19}F+^{208}Pb	105	1.35	0.285	2.0	1.320	0.15	1.37	81.51	12.74	8.3
^{16}O+^{144}Sm	100	1.295	0.365	4.0	1.250	0.15	1.1	60.25	11.46	10.0
^{16}O+^{62}Ni	75	1.333	0.380	6.0	1.250	0.33	1.04	30.41	10.2	7.78

3 Application

We apply the formulation developed in section 1.2 to the analysis of the collision data of eight typical heavy ion systems namely ^{12}C+^{208}Pb, ^{16}O+^{208}Pb, ^{19}F+^{208}Pb, , ^{16}O+^{144}Sm, and ^{16}O+^{62}Ni systems and obtain a unified and consistent description of the measured cross sections of elastic scattering and fusion, and the peculiar peak structure in the variation of the quantity $D(E_{c.m.})$=$\frac{d^2(E_{c.m.}\sigma_{fus})}{dE^2_{c.m.}}$ as a function of $E_{c.m.}$.

In the optical model potential (OMP) analysis of scattering of two nuclei of mass number A_1 and A_2 and proton numbers Z_1 and Z_2, the OMP is described by

$V(r) = -V_N f(r, R_V, a_V) - iW g(r, R_W, a_W) + V_C(r)$

in the entrance channel. The form factor used in this chapter is

$f(r, R, a) = g(r, R, a) = [1 + exp\{(r - R)/a\}]^{-1}$.

V_N and W are the strength of real and imaginary parts of OMP. The radius parameters are expressed as $r_V = R_V/(A_1^{1/3} + A_2^{1/3})$ and $r_W = R_W/(A_1^{1/3} + A_2^{1/3})$. The symbols a_V and a_W indicate diffuseness parameters. The Coulomb potential $V_C(r)$ is given by

$V_C(r) = \frac{Z_1 Z_2 e^2(3-r^2/R_C^2)}{2R_C},\ r \le R_C; V_C(r) = Z_1 Z_2 e^2/r,\ r > R_C,$

where $R_C = r_C(A_1^{1/3} + A_2^{1/3})$ with r_C as the Coulomb radius parameter. Thus, there are a total of seven parameters, V_N, r_V, a_V, W, r_W, a_W, and r_C, in this OMP.

3.1 Elastic-scattering cross section

The angular distribution of elastic scattering can be explained by a number of different sets of potential-descriptive parameters, according to what we know. All seven parameters in our current calculation are independent of energy, and when choosing the values for the potential, we were motivated by the fact that resonance can occur if the imaginary part W is weak and that such a weak absorption is sufficient if the real part is thought to be deep [40] and less diffused [41] to account for the elastic-scattering cross-section. In Table 1.1, the values of the OMP parameters used in the calculation for the analysis of elastic scattering data for the ^{12}C+^{208}Pb, ^{16}O+^{208}Pb, ^{19}F+^{208}Pb, ^{16}O+^{144}Sm , and ^{16}O+^{62}Ni, systems are given. Table 1.1 also contains the values of height V_B and radius R_B of the s-wave barrier for each of the above five systems.

(i) ^{12}C+^{208}Pb system

In the case of ^{12}C+^{208}Pb, according to the abovementioned prescription, the real portion is made deep with depth V_N = 125 MeV and less diffused with diffuseness parameter a_V = 0.32 fm and the radius parameter r_V =1.31 fm. The imaginary component also receives the additional parameters r_W =1.325 fm and a_W =0.25 fm, as well as a weak attractive strength of W=3.0 MeV. The Coulomb radius parameter is assumed to have a value of r_C = 0.9 fm. The real portion of the combined nuclear and Coulomb potentials for an s-wave can be shown in Fig. 1 as a function of radial distance for a visual illustration. This demonstrates the repulsive barrier for the ^{12}C+^{208}Pb system with height V_B= 56.7 MeV and position R_B= 12.16 fm lowering quickly in the inner side. According to the formulation, 'n' rectangular potentials, each with a width of 0.008 fm, are used to replicate the potential in the area $0 < r \le R_{max}$. The nuclear potential together with its imaginary portion is zero in the area $r > R_{max} \approx 15$ fm, leaving the effective potential as solely Coulombic with the centrifugal term. Using the S-matrix given by the expression (1.28), at

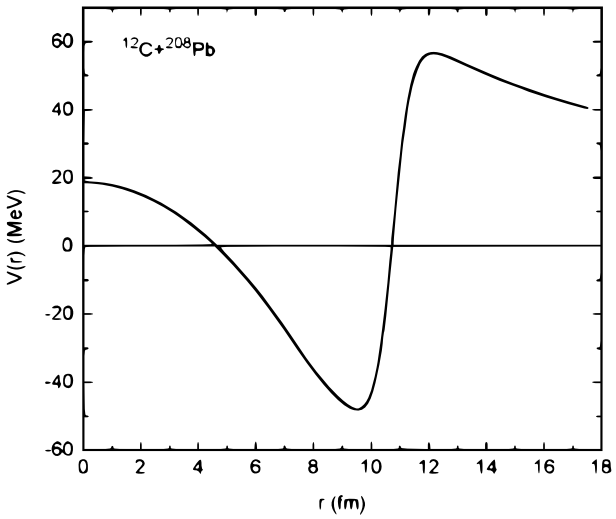

Figure 1: Plot of real part of nuclear plus Coulomb potentials for partial wave ℓ=0 as a function of radial distance with potential parameters V_0=-125 MeV, r_V=1.31 fm, a_V=0.32 fm, and r_C=0.9 fm for the ^{12}C+^{208}Pb system.

laboratory energies of 58.9, 60.9, 62.9, 64.9, 74.9, and 84.9 MeV, we get the findings of angular change of differential scattering cross-section. These computed findings are displayed in Fig. 2 as solid curves, and they are contrasted with the comparable experimental data from Ref. [1], which are depicted in the same figure as solid circles.

It is obvious that the data explanation in each energy case is fairly sound. It should be noted that we utilized the exact same set of OMP values listed in Table 1.1 to explain the results for all energies between 58.9 MeV and 84.9 MeV. In other words, OMP parameter values are independent of energy. We should also point out that the value of r_C = 0.9 fm that we are considering is a little lower than the standard value of r_C = 1.25 fm. This fact is supported by the calculation's conclusion in Ref. [42] about Coulomb potentials in heavy ion interactions, which shows that it has no impact on the outcomes of the elastic-scattering cross-section in our calculation. This lower value of r_CrC has been utilized to consistently account for the fusion cross-section data at low energy for the ^{12}C+^{208}Pb system that will be covered in the next section.

(ii) ^{16}O+^{208}Pb system

We have taken into consideration a deep real potential in this instance as well, with depth V_N = 125 MeV and a small diffuseness parameter a_V = 0.285 fm. Other parameter values are shown in Table 1.1. The barrier lowering steeply in the inner side with height V_B=73.7 MeV and radius R_B=12.52 fm for this system can be seen in the plot of the real component of nuclear plus Coulomb potentials as a function of radial distance for s-wave in Fig. 3.

Figure 4 shows a comparison between our projected differential scattering cross-section values (solid curves) and the corresponding experimental data (solid circles) from Reference [2] at various laboratory energies, including 80, 83, 88, 90, 96, and 102 MeV. It is obvious that the data's explanation for all energies is sound. Additionally, we have employed a single potential for all energies in this case, but with a lesser value of $r_C = 1.02$ fm.

(iii) ^{19}F+^{208}Pb system

In this system, we have taken a deep real potential with depth V_N=105 MeV and a small diffuseness parameter a_V=0.285 fm. Values of other parameters are given in Table 1.1. Using the S-matrix given by equation (1.28), we obtain the results of angular variation of differential scattering cross section at laboratory energies, 88.0, 91.0, 93.0, 96.0, 98.0, and 102.0 MeV. In Fig. 5, these computed results are depicted as solid curves, and they are compared with the analogous experimental data from [6], which are displayed as solid circles in the same figure. It is obvious that the data's explanation for all energies is reasonable.

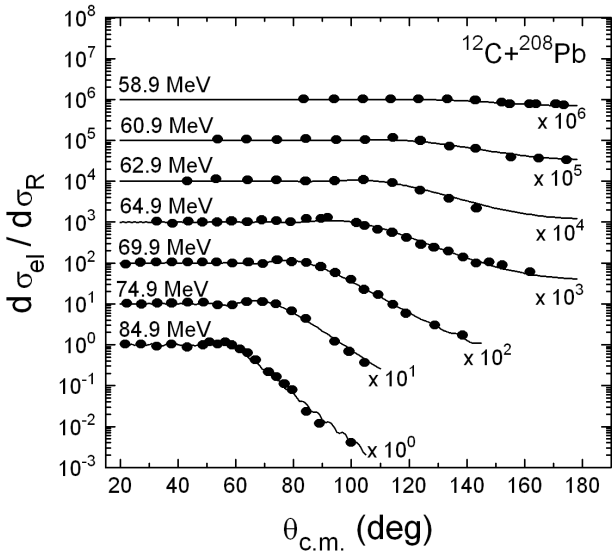

Figure 2: Angular distribution of elastic scattering cross sections (ratios to Rutherford) of ^{12}C+^{208}Pb system at laboratory energies 58.9, 60.9, 62.9, 64.9, 69.9, 74.9, and 84.9 MeV as a function of $\theta_{c.m.}$. The full drawn curves are theoretical results of present optical model calculation. The solid circles are experimental data taken from [1].

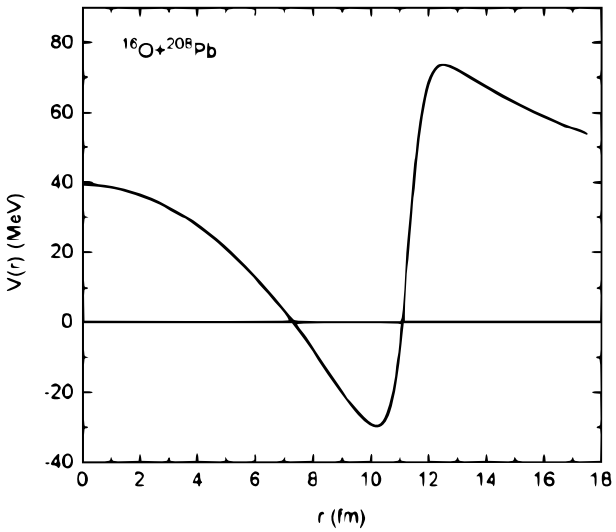

Figure 3: Plot of real part of nuclear plus Coulomb potentials for partial wave ℓ=0 as a function of radial distance with potential parameters V_0=-125 MeV, r_V=1.339 fm, a_V=0.285 fm, and r_C=1.02 fm for the ^{16}O+^{208}Pb system.

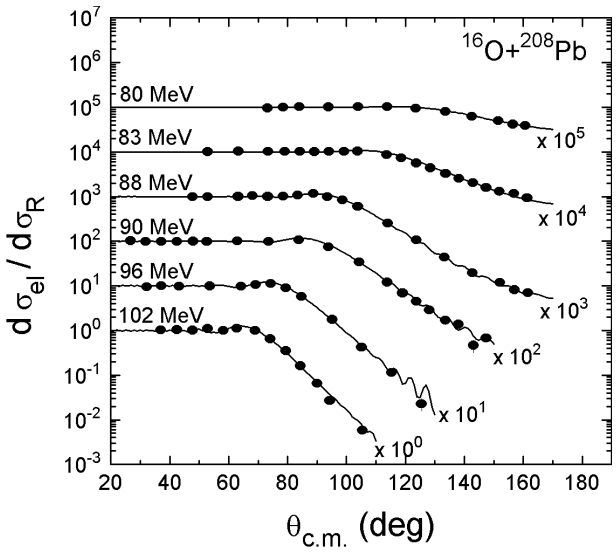

Figure 4: Same as Fig. 2 for ^{16}O+^{208}Pb system at laboratory energies 80, 83, 88, 90, 96, and 102 MeV. The full drawn curves are theoretical results of present optical model calculation. The solid circles are experimental data taken from [2].

(v) ^{16}O+^{144}Sm system

Similar calculations are done for this system. We have chosen a deep real potential with V_N = 100.0 MeV and a minimal diffuseness value of a_V = 0.365 fm in this case as well. Other parameter values are shown in Table 1.1. Figure 6 compares the calculated differential scattering cross-section values (solid curves) with the corresponding experimental data (solid circles) from Reference [8] at various energies, 66.0, 69.2, and 72.3 MeV. It is seen that the agreement with experimental data is quite good.

(vii) ^{16}O+^{62}Ni system

Here, we have used the optical potential parameters of ^{16}O+^{58}Ni system except r_V=1.333 fm. In Fig. 7, we compare the computed differential scattering cross-section findings (solid curves) with corresponding experimental data (solid circles) obtained from references [11] at various energies 42.0, 48.0 and 54.0 MeV. It is clear from the figure that the above experimental data are successfully reproduced by our method simultaneously.

In light of the necessity that such potential is essential in the description of fusion data to be carried out below for the aforementioned eight systems, finding of such energy independent OMP is a significant conclusion of this research.

3.2 Fusion cross section

Fusion of the two nuclei is a crucial mechanism that is actively linked to the elastic scattering event in the low-energy collision process. It is simple to take into account that the fusion cross section, σ_{fus}, is a portion of the overall reaction cross section, σ_r, when estimating cross sections for elastic scattering and fusion simultaneously. However, it is never easy to take a part from σ_r that precisely accounts for the observed results of fus at different incidence energy across a large range. In order to compute σ_{fus}, we take into account the DRM of Udagawa et al. [14]. The quantity of absorption cross section inside the inner zone $0 < r < R_{fus}$ is what this model refers to as the fusion cross section. Where R_{fus} is a radial distance expected to be less than R_B which is the radial position of the s-wave Coulomb barrier in the case of a given nucleus-nucleus system. In the formulation through Eq.

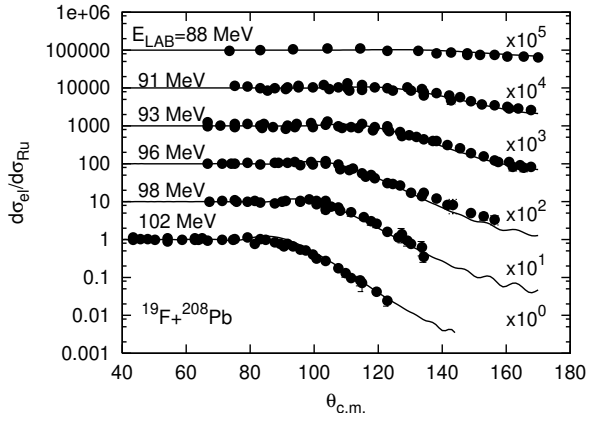

Figure 5: Angular distribution of elastic scattering cross sections (ratios to Rutherford) as a function of $\theta_{c.m.}$ of ^{19}F+^{208}Pb system at different laboratory energies. The full drawn curves are theoretical results of our optical model calculation. The solid circles are experimental data taken from [6].

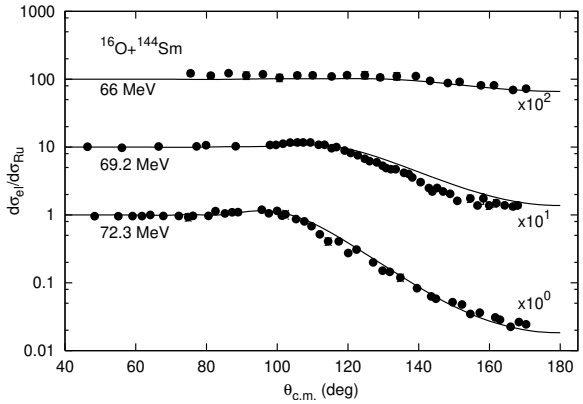

Figure 6: Angular distribution of elastic scattering cross sections (ratios to Rutherford) as a function of $\theta_{c.m.}$ of ^{16}O+^{144}Sm system at different laboratory energies. The full drawn curves are theoretical results of our optical model calculation. The solid circles are the experimental data taken from [8].

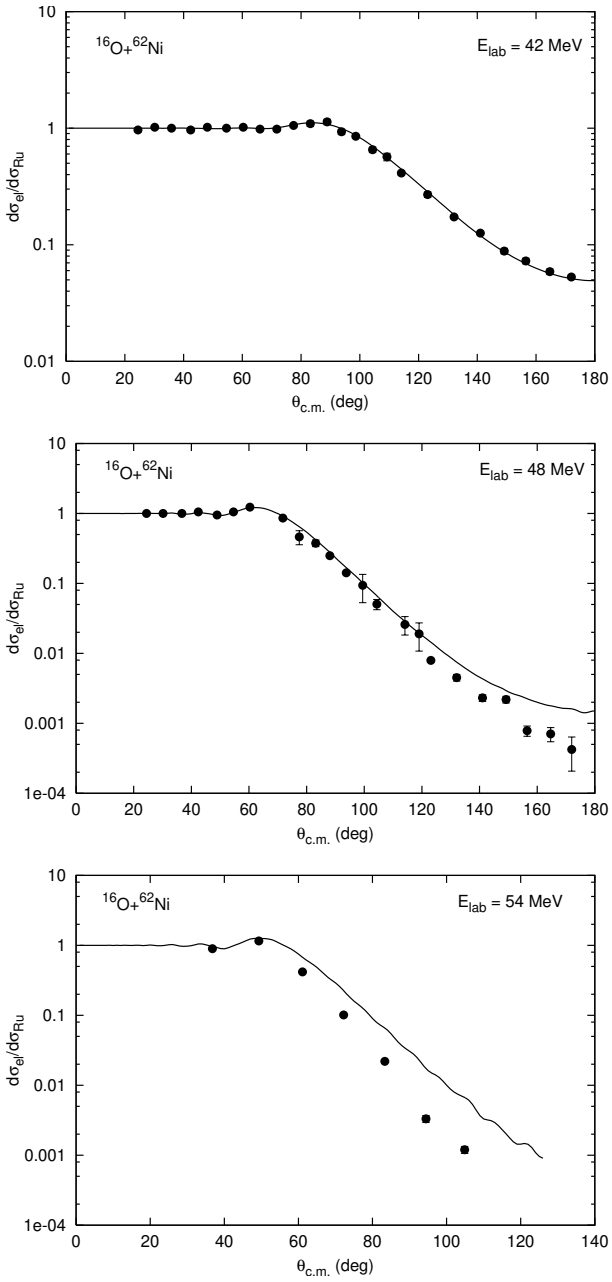

Figure 7: Angular distribution of elastic scattering cross sections (ratios to Rutherford) as a function of $\theta_{c.m.}$ of ^{16}O+^{62}Ni system at different laboratory energies. The full drawn curves are theoretical results of our optical model calculation. The solid circles are experimental data taken from [11].

(1.34), we have calculated the values of σ_{fus} as per the above principle of DRM.

(i) ^{12}C+^{208}Pb system

Using R_{fus}=9.9 fm, we obtain the results of σ_{fus} for the ^{12}C+^{208}Pb system and compare it (solid curve) in Fig. 8 with the corresponding experimental data (solid circles) taken from Ref. [3]. It is obvious that the data matching throughout the whole energy range, from $E_{c.m.}$=50 MeV to 75 MeV, is pretty excellent. The OMP parameters whose values explain the elastic scattering data in Fig. 2 have not been altered in order to achieve this fitting. The values of R_{fus}= 9.9 fm utilized in our computation are smaller than the value of Coulomb radius R_B=12.16 fm in this system, which is required by the permissible state of reality. Further, the importance of the present successful description of elastic scattering and fusion cross sections increases due to the observation [3, 26] that there is systematic failure of the Woods-Saxon nuclear potential describing these data, simultaneously.

(ii) ^{16}O+^{208}Pb system

Similarly remarkable accomplishment is attained in the case of the ^{16}O+^{208}Pb system, where our calculated results (complete curve) are able to match the experimental data (solid dot) of σ_{fus} taken from Ref. [4] across the whole range of energy from $E_{c.m.}$=68 MeV to 86 MeV. The fusion radius in this instance, R_{fus}=8.8 fm, is less than the Coulomb radius, R_B=12.52 fm. Unlike in the case of ^{12}C+^{208}Pb, in this ^{16}O+^{208}Pb system, we need to slightly modify the value of the nuclear radius parameter r_V=1.35 fm (Table 1.1) used in the analysis of scattering data and take r_V=1.339 fm for the fitting of measured σ_{fus} data.

(iii) ^{19}F+^{208}Pb system

In this case, we have used the fusion radius R_{fus}=8.3 fm which is less than the Coulomb radius R_B=12.74 fm. In Fig. 10, we compare our calculated results (solid curves) of fusion cross section with the corresponding experimental data (solid circles) taken from Ref. [7]. In order to get a good fitting in fusion cross section, we need to slightly modify the nuclear radius parameter r_V=1.35 fm used in the analysis of elastic scattering to r_V=1.356 fm.

(v) ^{16}O+^{144}Sm system

When our calculated results (full curve) are compared to the experimental data (solid dot) of σ_{fus} taken from Ref. [9] for the ^{16}O+^{144}Sm system shown in Fig. 11, a similar result is achieved. The fusion radius in this instance, R_{fus}=10.0 fm, is less than the Coulomb radius, R_B=11.46 fm. The nuclear radius parameter, r_V, which was previously set to 1.145 fm (Table 1.1) for the analysis of scattering data must now be changed to 1.295 fm for the fitting of observed σ_{fus} data.

(vii) ^{16}O+^{62}Ni system

Here, we have taken R_{fus}=7.78 fm which is less than R_B=10.20 fm. The calculated results (solid curve) of fusion cross section is compared with the experimental data (solid circles) taken from Ref. [11] in Fig. 12. It is clear from the figure that the

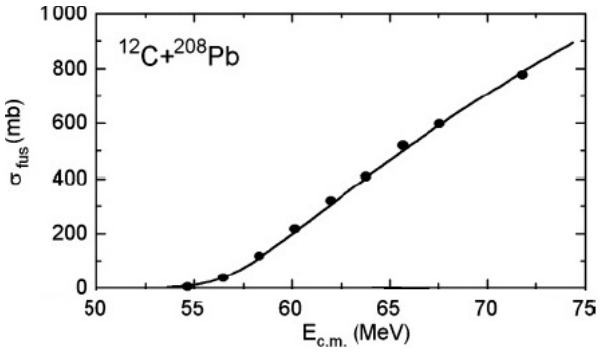

Figure 8: Variation of fusion cross section σ_{fus} as a function of energy $E_{c.m.}$ for the ^{12}C+^{208}Pb system. The full curve represents our calculated results. The experimental data shown by solid circles are obtained from [3].

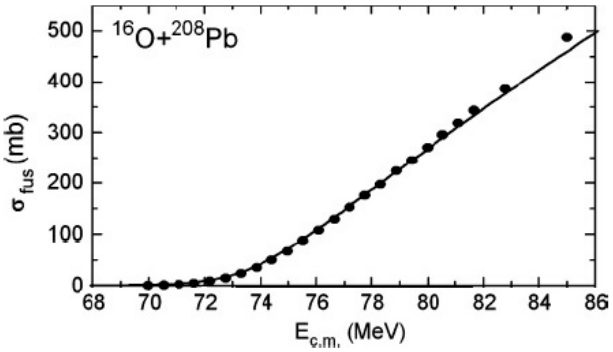

Figure 9: Variation of σ_{fus} as a function of $E_{c.m.}$ for the ^{16}O+^{208}Pb system. The full curve represents our calculated results. The experimental data shown by solid circles are obtained from [4].

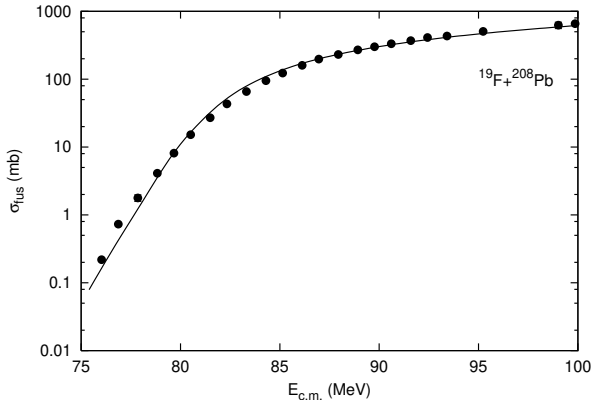

Figure 10: Variation of fusion cross section σ_{fus} as a function of energy $E_{c.m.}$ for the ^{19}F+^{208}Pb system. The full curve represents our calculated results. The experimental data shown by solid circles are obtained from [7].

theoretical results is in excellent agreement with the experimental data. To achieve this we have slightly changed the r_V value from 1.333 fm (used for elastic scattering calculation) to 1.313 fm.

The fusion radius R_{fus} values we utilized in our calculations are, however, smaller in all of these systems than the corresponding Coulomb radius R_B values. This indicates unequivocally that fusion is an internal phenomena whereas scattering and other distant, less absorptive direct reaction mechanisms are responsible for the surface occurrence. We should note that for a given system, there may be many sets of possible Woods-Saxon parameters that describe elastic scattering data in a manner that is comparable. Since elastic scattering is a surface phenomenon, all sets of potential parameter sets produce Coulomb barriers with the same height V_B and fixed radial position R_B, but different sets produce different depths and slopes of the effective potential on the interior side $r < R_B$. However, the fusion of two nuclei is an internal phenomenon that is defined by absorption in this area, and the values of the radius parameter R_{fus}, which is located in the region $0 < r < R_B$, are responsible for the corresponding cross-section. The value of R_{fus} will be determined by the set of potential parameters employed in the study of scattering, hence it may have different values for various sets of potential. We need not, however, alter the value of R_{fus} as a function of energy for the study of σ_{fus} at various incidence energies as we have chosen a single potential for the description of both elastic and fusion cross sections. R_{fus}'s energy-independent character is essential since it makes the product $E_{c.m.}\sigma_{fus}$ energy derivative simpler in the results of $\frac{d^2(E_{c.m.}\sigma_{fus})}{dE^2}$ which is described in the next sub-section.

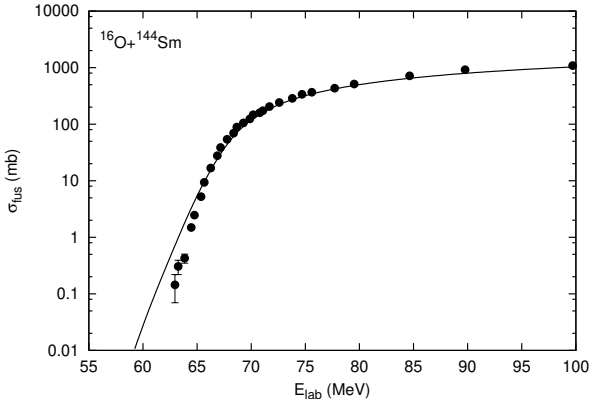

Figure 11: Variation of fusion cross section σ_{fus} as a function of energy E_{lab} for the ^{16}O+^{144}Sm system. The full curve represents our calculated results. The experimental data shown by solid circles are obtained from [9].

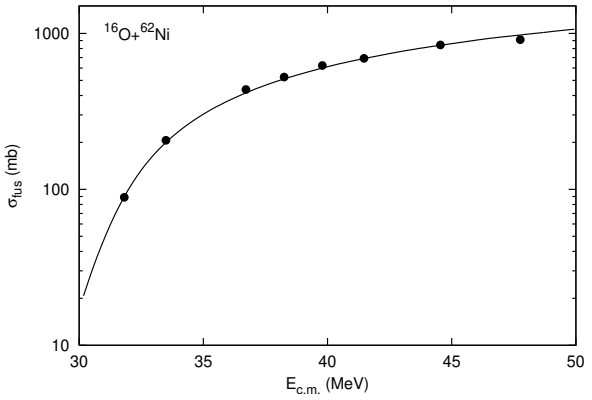

Figure 12: Variation of fusion cross section σ_{fus} as a function of energy $E_{c.m.}$ for the ^{16}O+^{62}Ni system. The full curve represents our calculated result. The experimental data shown by solid circles are obtained from [11].

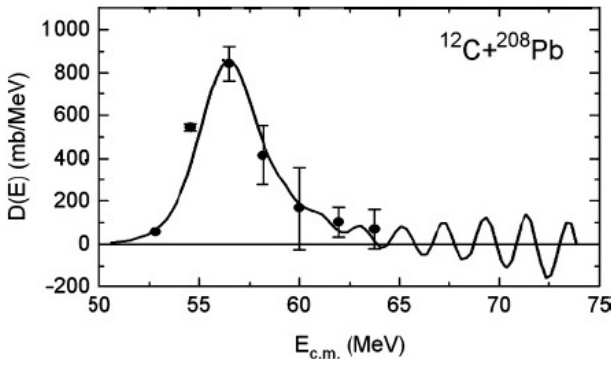

Figure 13: Variation of $D(E_{c.m.})$=$\frac{d^2(E_{c.m.}\sigma_{fus})}{dE^2_{c.m.}}$ as a function of energy $E_{c.m.}$ corresponding to results of σ_{fus} for ^{12}C+^{208}Pb system. The full curve represents our calculated result. The experimental data shown by solid circles are obtained from [3].

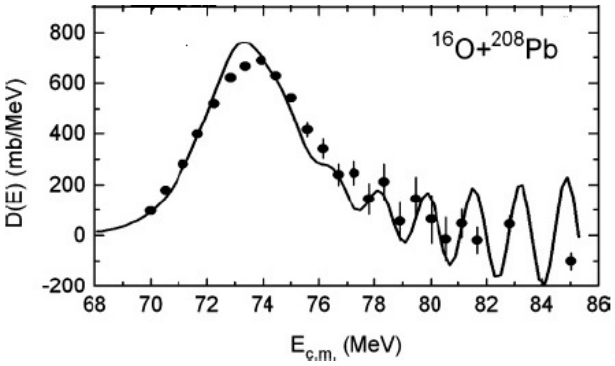

Figure 14: Variation of $D(E_{c.m.})$=$\frac{d^2(E_{c.m.}\sigma_{fus})}{dE^2_{c.m.}}$ as a function of energy $E_{c.m.}$ corresponding to results of σ_{fus} in ^{16}O+^{208}Pb system. The full curve represents our calculated result. The experimental data shown by solid circles are obtained from [4].

3.3 Explanation of D(E$_{c.m.}$)

The results of σ_{fus} from experiment and theory as a function of energy, as shown in Figs. (8 to 12), do not exhibit any kind of structure. Therefore, nothing further can be inferred about the potential physical incidents that could be contributing to the fusion process from this logical interpretation of the monotonically evolving data. The identical result of σ_{fus} is reported in a different way as follows in order to provide some insight into these processes. One can extract values of a quantity that is the second derivative of the product $E_{c.m.}\sigma_{fus}$ denoted by $D(E_{c.m.})$=$\frac{d^2(E_{c.m.}\sigma_{fus})}{dE^2_{c.m.}}$ with respect to energy $E_{c.m.}$. For this, the following point difference formula can be used:

$$D(E) = \big[(E-\Delta E)\sigma_- - 2E\sigma + (E+\Delta E)\sigma_+\big]/(\Delta E)^2, \tag{35}$$

where σ_-, σ, and σ_+ indicate fusion cross sections σ_{fus} at center of mass energies $E-\Delta E$, E and $E+\Delta E$, respectively, with energy step size ΔE. Function $D(E_{c.m.})$ is generally referred to as barrier distribution [5, 9, 43].

We get the amount $D(E_{c.m.})$ as a function of $E_{c.m.}$Ec.m. from our computed results of σ_{fus} using the formula (1.35). For the ^{12}C+^{208}Pb system, we present our results in Fig. 13 as a solid curve and then compare them with the relevant experimental data (solid circles). It can be observed that our calculation accurately reproduces the major peak as well as a few other minor peaks in the higher energy range.

Similarly, in Figs. 14, 16, and 17 we obtain remarkable matching of the highly oscillatory structures of the measured data of $D(E_{c.m.})$ in the cases of ^{16}O+^{208}Pb, ^{19}F+^{208}Pb, ^{16}O+^{92}Zr, ^{16}O+^{144}Sm, ^{16}O+^{62}Ni, and ^{6}Li+^{209}Bi systems respectively.

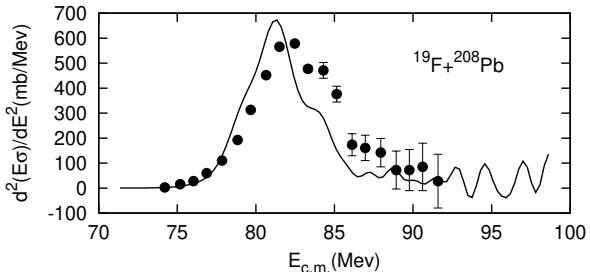

Figure 15: Variation of $D(E_{c.m.})$=$\frac{d^2(E_{c.m.}\sigma_{fus})}{dE^2_{c.m.}}$ as a function of energy $E_{c.m.}$ corresponding to results of σ_{fus} for ^{19}F+^{208}Pb system. The full curves represent our calculated results. The experimental data shown by solid circles are obtained from [7].

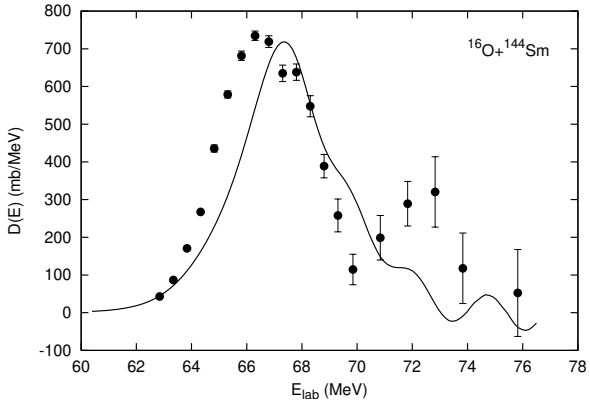

Figure 16: Variation of $D(E)$ as a function of energy E_{lab} corresponding to results of σ_{fus} for ^{16}O+^{144}Sm system. The full curve represents our calculated result. The experimental data shown by solid circles are obtained from [10].

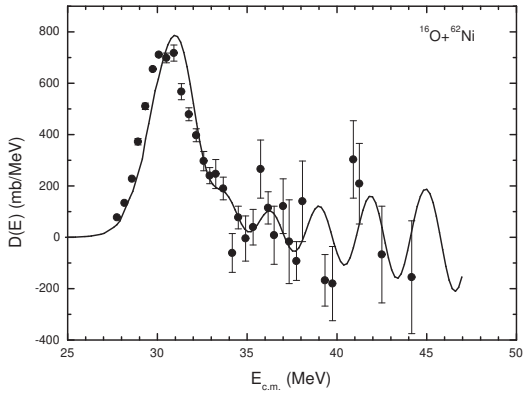

Figure 17: Variation of $D(E_{c.m.})$=$\frac{d^2(E_{c.m.}\sigma_{fus})}{dE^2_{c.m.}}$ as a function of energy $E_{c.m.}$ corresponding to results of σ_{fus} for ^{16}O+^{62}Ni system. The full curve represents our calculated result. The experimental data shown by solid circles are obtained from [12].

More crucially, the unfavourable character of some of the dips in the higher-energy zone is fairly clearly explained. The discovery [4] that the more microscopic coupled channel calculation [44] for fusion has failed to explain the results of $D(E_{c.m.})$ in the ^{16}O+^{208}Pb system [4,23] raises the significance of this successful explanation. It's worth noting that there are three ways to disrupt the oscillatory structures in all of the systems mentioned above; : (i) by increasing the imaginary component W's strength; (ii) by taking into account a higher Coulomb radius parameter r_C; and (iii) by increasing the step size ΔE for differentiation using formula (1.35). In order to provide an appropriate explanation for the elastic scattering data as well as an explanation for the observed results of σ_{fus} and $D(E_{c.m.})$., the values of W and r_C are fixed.

4 Summary and conclusion

Analytical solutions to the Schrödinger equation with composite optical potential of two interacting nuclei result in a recursive mathematical formula for the scattering matrix. An analytical formula for the absorption cross-section has been established to take into consideration the reaction cross-sectionsection using the same potential and wave function. The formulation is applied to the ^{12}C+^{208}Pb, ^{16}O+^{208}Pb, ^{19}F+^{208}Pb, ^{16}O+^{144}Sm , and ^{16}O+^{62}Ni systems for the analysis of the following experimental data in a consistent manner. (i) The angular fluctuations of the cross-section of differential scattering at various energies near the Coulomb barrier. (ii) Fusion cross-section σ_{fus} as a function of energy throughout a large range spanning the Coulomb barrier area. (iii) The outcome of the quantity $D(E_{c.m.})$=$\frac{d^2(E_{c.m.}\sigma_{fus})}{dE^2_{c.m.}}$.

The key characteristics that result from this analysis may be summed up as follows.
(a) The elastic-scattering data at various energies could be well explained by a single, complex nuclear potential in Woods-Saxon form without any energy dependency. Important characteristics of the complex optical potential employed in the computation include large depth and little diffuseness in the real part and weak strength (low absorption) in the imaginary component.
(b) A key component of the computation is the estimation of the reaction cross-sectional area that will be used to calculate the fusion cross-section using the stepwise absorption approach. This procedure of dividing up the overall reaction cross-section is natural in the sense that neither the extraction process nor the division of the imaginary part ever requires additional energy.
(c) The results of σ_{fus} presented in another form namely $D(E_{c.m.})$=$\frac{d^2(E_{c.m.}\sigma_{fus})}{dE^2_{c.m.}}$ by using point difference formula show peculiar peak structure in its variation with $E_{c.m.}$. Our calculated outcomes for σ_{fus} presented in the aforementioned manner describe this outcome with highs and lows with a surprising degree of success.
(d) It has been found that resonance states can develop when two nuclei collide because of the optical potential's weakly absorptive property indicated in item (a) above. Following that, it comes out that these resonances regulate the oscillatory or peak structure of $D(E_{c.m.})$ mentioned in point (c) above.

References

[1] S. Santra, P. Singh, S. Kailas, A. Chatterjee, A. Shrivastava, and K. Mahata, *Phys. Rev.* **C 64**, 024602 (2001).

[2] F. Videbaek, R. B. Goldstein, L. Grodzins, S. G. Steadman, T. A. Belote, and J. D. Garrett, *Phys. Rev.* **15**, 954 (1977).

[3] A. Mukherjee, D. J. Hinde, M. Dasgupta, K. Hagino, J. O. Newton, and R. D. Butt, *Phys. Rev.* **C 75**, 044608 (2007).

[4] C. R. Morton, A. C. Berriman, M. Dasgupta, D.J. Hinde, J.O. Newton, K. Hagino, and I.J. Thompson, *Phys. Rev.* **C 60**, 044608 (1999).

[5] M. Dasgupta, D. J. Hinde, N. Rowley, and A. M. Stefanini, *Annu. Rev. Part. Sci.* **48**, 401 (1998), and references therein.

[6] C. J. Lin, J. C. Xu, H. Q. Zhang, Z. H. Liu, F. Yang, and L. X. Lu, *Phys. Rev.* **C 63** 064606 (2001).

[7] D. J. Hinde, A. C. Berriman, M. Dasgupta, J. R. Leigh, J. C. Mein, C. R. Morton, and J. O. Newton, *Phys. Rev.* **C 60** 054602 (1999).

[8] D. Abriola, D. DiGregorio, J. E. Testoni, A. Etchegoten, J. O. Fernandez, A. M. J. Ferrero, S. Gil, A. O. Macchiavelli, A. J. Pacheco, and J. Kittl, *Phys. Rev.* **C 39** 546 (1989).

[9] J. R. Leigh, M. Dasgupta, D. J. Hinde, J. C. Mein, C. R. Morton, R. C. Lemmon, J. P. Lestone, J. O. Newton, H. Timmers, J. X. Wei, and N. Rowley, *Phys. Rev.* **C 52**, 3151 (1995).

[10] K. Hagino, N. Takigawa, and S. Kuyucak, *Phys. Rev. Lett.* **79** 2943 (1997).

[11] N. Keeley, J. A. Christly, N. M. Clarke, B. R. Fulton, J. S. Lilley, M. A. Nagarajan, I. J. Thompson, *Nucl. Phys.* **A582** 314 (1995).

[12] N. Keeley, J. S. Lilley, J. X. Wei, M. Dasgupta, D. J. Hinde, J. R. Leigh, J. C. Mein, C. R. Morton, H. Timmers, and N. Rowley, *Nucl. Phys.* **A628** 1 (1998).

[13] Y. Eisen and Z. Vager, *Nucl. Phys.* **A 187**, 219 (1972).

[14] T. Udagawa, B. T. Kim, and T. Tamura, *Phys. Rev.* **C 32**, 124 (1985).

[15] T. Udagawa, S. -W. Hong, and T. Tamura, *Phys. Rev.* **C 32**, 1435 (1985).

[16] J. R. Birkelund and J. R. Huizenga, *Annu. Rev. Nucl. Part. Sci.* **33**, 265 (1983).

[17] S. G. Steadman and M. J. Rhoades-Brown, *Anuu. Rev. Nucl. Part. Sci.* **36**, 649 (1986).

[18] G. R. Satchler, M. A. Nagarajan, J. S. Lilley, and I. J. Thompson, *Phys. Rev.* **C 41**, 1869 (1990).

[19] M. A. Nagarajan and G. R. Satchler, *Phys. Lett.* **B173**, 29 (1986).

[20] C. H. Dasso and S. Landowne, *Comput. Phys. Commun.* **46** (1987) 187; M. Dasgupta, A. Navin, Y. K. Agrawal, C. V. K. Baba, H. C. Jain, M. L. Thingan, and A. Roy, *Nucl. Phys.* **A 539**, 351 (1992).

[21] I. J. Thompson, *Comput. Phys. Rep.* **7**, 167 (1998).

[22] K. Hagino, N. Rowley, and A. T. Kruppa, *Comput. Phys. Commun.* **123**, 143 (1999).

[23] Henning Esbensen and Serban Misicu, *Phys. Rev.* **C 76**, 054609 (2007).

[24] M. Dasgupta, D. J. Hinde, A. Diaz-Torres, B. Bouriquet, Catherine I. Low, G. J. Milburn, and J. O. Newton, P̂hys. Rev. Lett. **99**, 192701 (2007).

[25] R. N. Sagaidak, S. P. Tretyakova, S. V. Khlebnikov, A. A. Ogloblin, N. Rowley, and W. H. Trzaska, *Phys. Rev.* **C 76**, 034605 (2007).

[26] J. O. Newton, R. D. Butt, M. Dasgupta, D. J. Hinde, I. I. Gontchar, C. R. Morton, and K. Hagino, *Phys. Rev.* **C 70**, 024605 (2004).

[27] D. J. Hinde, M. Dasgupta, C. R. Morton, A. C. Berriman, R. D. Butt, and J. O. Newton, *Nucl. Phys.* **A 654**, 864c (1999); D. J. Hinde, C. R. Morton, M. Dasgupta, J. R. Leigh, J. C. Mein, and H. Timmers, *Nucl. Phys.* **A592**, 271 (1995).

[28] M. R. Spinella, J. E. Testoni, O. Dragun, and H. D. Matra, *Nucl. Phys.* **A687**, 385 (2001).

[29] G. R. Satchler, M. A. Nagarajan, J. S. Lilley, and I. J. Thompson, *Ann. Phys.* **178**, 110 (1987).

[30] M. L. Halbert, J. R. Beene, D. C. Hensley, K. Honkanen, T. M. Semkow, V. Abenante, D. G. Sarantites, and Z. Li, *Phys. Rev.* **C 40**, 2558 (1989).

[31] Basudeb Sahu, G. S. Mallick, B. B. Sahu, S. K. Agarwalla and C. S. Shastry, *Phys. Rev.* **C 77**, 024604 (2008).

[32] R. R. Swain, C. Dash, P. Mohanty, B.B. Sahu *Int. J. Mod.* **E 29**, 2050016 (2020).

[33] C.Dash, R. R. Swain, G. Tripathy, I. Naik, B. B. Sahu. *Chinese Physics* **C 46**, 124104-1-8, (2022).

[34] R. H. Landau and M. J. P. Mejia, *Computational Physics* (John Wiley and Sons, New york, 1997).

[35] F. R. Loscalzo and T. D. Talbot, *Bull. Amer. Math. Soc.* **73**, 438 (1967).

[36] G. Micula, *Math. Comp.* **27**, 807 (1973).

[37] Basudeb Sahu, Bidhubhusan Sahu, and Santosh K. Agarwalla, *Pramana: J. Phys.* **70** (2007) 27.

[38] M. A. Melkanoff, T. Sawada, and J. Raynal, *Methods in Computational Physics, Vol. VI, Nuclear Optical Model Calculations* (Academic Press, New York, 1966).

[39] C. S. Shastry and Y. K. Gambhir, *Phys. Rev.* **C 28**, 1109 (1983).

[40] M. P. Nicoli, F. Haas, R. M. Freeman, N. Aissaoui, C. Beck, A. Elanique, R. Nouicer, A. Morsad, S. Szilner, Z. Basrak, M.E. Brandan, and G.R. Satchler, *Phys. Rev.* **C 60**, 064608 (1999).

[41] S. C. Pieper, M. J. Rhoades-Brown, and S. Landowne, *Phys. Lett.* **B162**, 43 (1985).

[42] R. M. Devries and M. R. Clover, *Nucl. Phys.* **A243**, 528 (1975).

[43] A. B. Balantekin and N. Takigawa, *Rev. Mod. Phys.* **70**, 77 (1998).

[44] N. Rowley, G. R. Satchler, and P.H. Stelson, *Phys. Lett.* **B254**, 25 (1991).

[45] B. Sahu, L. Satpathy, and C. S. Shastry, *Phys. Lett.* **A303**, 105 (2002).

[46] B. Sahu, S. K. Agarwalla, and C. S. Shastry, *Nucl. Phys.* **A713**, 45 (2003).